

CrossMark
click for updates

Cite this: DOI: 10.1039/c4ta06111j

A single-material graded refractive index layer for improving the efficiency of III–V triple-junction solar cells

Chan Il Yeo,^a Hee Ju Choi,^b Young Min Song,^c Seok Jin Kang^d and Yong Tak Lee^{*ad}

We present a single-material titanium oxide (TiO₂) bi-layer antireflection coating (ARC) produced using oblique angle deposition for improving the power conversion efficiency (PCE) of III–V compound semiconductor triple-junction (TJ) solar cells. Experimental demonstration of the porous TiO₂ layers and optical modelling by rigorous coupled-wave analysis indicate that bi-layer TiO₂ could be used as universal ARC for all known TJ stacks with various material combinations. The optimum TiO₂ bi-layer ARC produced on a Ga_{0.5}In_{0.5}P/GaAs/Ge TJ solar cell exhibits considerably enhanced PCE of 31.6%, which is higher than that of the cells without ARC (23.8%) and with TiO₂ single-layer ARC (29.1%). Incident angle-dependent device characteristics of the fabricated TJ solar cells are also discussed.

Received 12th November 2014

Accepted 2nd February 2015

DOI: 10.1039/c4ta06111j

www.rsc.org/MaterialsA

Introduction

III–V semiconductor based multi-junction (MJ) solar cells are promising candidates for achieving high power conversion efficiency (PCE) and for solar power plants and space applications due to their broadband absorption and strong durability.^{1–5} A great deal of effort has been put into improving the PCE of III–V semiconductor MJ solar cells. To achieve high PCE, fundamentally, high photon absorption over the entire absorption spectrum of the solar cells is particularly essential. However, high Fresnel reflection losses originating from the large refractive index difference between air and the semiconductor material causes fewer photons to be transmitted into the solar cell.^{4,6} In addition, photocurrent matching between series connected subcells, which is one of the most challenging issues in MJ solar cells, is crucial for improving their PCE.^{1–4} This is because the net photocurrent of the MJ solar cell is determined by the subcell with the smallest photocurrent among the series connected subcells. To address this issue, finely designed surface antireflective structures have been investigated, which take into account the absorption spectrum of each subcell and the solar irradiance. This approach can effectively enhance the net photocurrent in the MJ solar cells and thereby improve the PCE. Commonly, multi-layer

antireflection coatings (ARCs) with different optical materials have been widely used for surface antireflection. However, it has fatal drawbacks of very limited materials with suitable refractive indices and thermal mismatch.⁷ Since there are no standard MJ stacks, material selection issues are critical to the design and optimization of MJ solar cells.

Herein, we propose the use of versatile, single-material bi-layer ARCs with different refractive indices for improving the absorption efficiency of MJ solar cells. Porous titanium dioxide (TiO₂) bi-layers with different refractive indices were prepared by oblique angle deposition (OAD)^{8–13} and directly employed on top of III–V semiconductor TJ solar cells with stacks of Ga_{0.5}In_{0.5}P/GaAs/Ge. The device performances (reflectance, cell efficiency, angle dependency, *etc.*) were systematically investigated. The experimental results and theoretical modelling of a TiO₂ bi-layer with different porosities showed that it is applicable to three ‘representative’ types of high-efficiency III–V semiconductor triple-junction (TJ) solar cells, *i.e.*, Ga_{0.5}In_{0.5}P/GaAs/Ge, Ga_{0.51}In_{0.49}P/Ga_{0.96}In_{0.04}As/Ga_{0.37}In_{0.63}As, and Ga_{0.35}In_{0.65}P/Ga_{0.83}In_{0.17}As/Ge TJ solar cells.¹

Experimental and simulation modelling details

Fig. 1(a) shows a schematic illustration of a TJ solar cell with a TiO₂ bi-layer consisting of porous and dense TiO₂ films. The purpose of the bi-layer is to reduce unwanted surface reflection loss by introducing a graded refractive index ARC onto the outermost layer material (*i.e.*, Aluminium Indium Phosphide, AlInP) of the solar cell. In this study, TiO₂ was deliberately employed as an optical material for ARC because it has a relatively high refractive index among various optical

^aAdvanced Photonics Research Institute, Gwangju Institute of Science and Technology, 1 Oryong-dong, Buk-gu, Gwangju, 500-712, Republic of Korea. E-mail: ytleee@gist.ac.kr; Fax: +82-62-715-3128; Tel: +82-62-715-2278

^bDepartment of Physics and Photon Science, Gwangju Institute of Science and Technology, 1 Oryong-dong, Buk-gu, Gwangju, 500-712, Republic of Korea

^cDepartment of Electronics Engineering, Pusan National University, 2 Busandaehak-ro 63beon-gil, Geumjeong-gu, Busan, 609-735, Republic of Korea

^dSchool of Information and Communications, Gwangju Institute of Science and Technology, 1 Oryong-dong, Buk-gu, Gwangju, 500-712, Republic of Korea

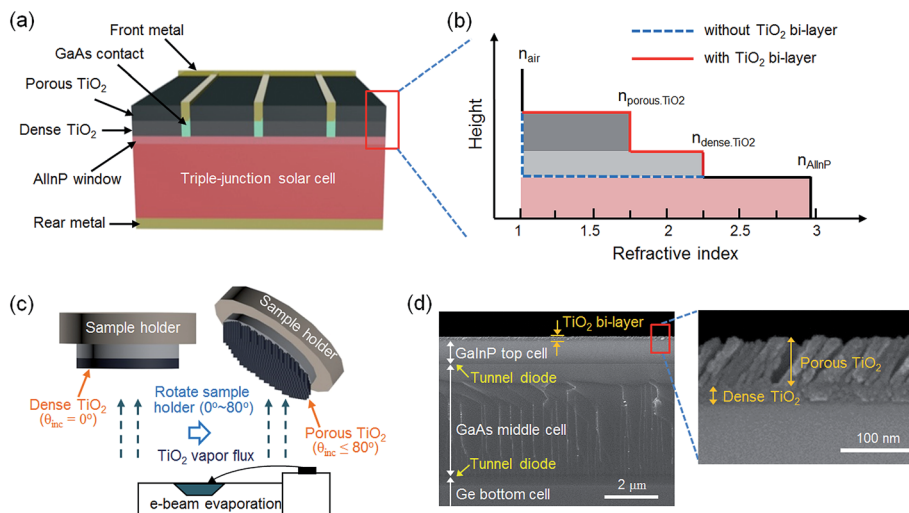


Fig. 1 (a) Schematic illustration of the TJ solar cell with the TiO_2 bi-layer. (b) Refractive index profiles of TJ solar cells without and with the TiO_2 bi-layer. Refractive indices of each material at ~ 600 nm are considered. (c) Schematic of OAD of TiO_2 films. (d) SEM image of the GaInP/GaAs/Ge TJ solar cell with TiO_2 bi-layer ARC.

materials, which is a good feature for producing a graded refractive index ARC with a small difference in refractive index at the interface between the ARC and III-V semiconductor solar cells. In addition, TiO_2 is a highly transparent, nontoxic, and chemically and mechanically stable material.¹⁴ TiO_2 ARC can be simply fabricated using general methods such as evaporation and sputtering of the TiO_2 source as well as spin-coating of a colloidal solution containing TiO_2 nanoparticles.^{14,15} Refractive index profiles of the TJ solar cells without and with the TiO_2 bi-layer ARC are shown in Fig. 1(b). It is clearly seen that the abrupt refractive index change from air ($n_{\text{air}} = 1$) to the outermost layer material of the TJ solar cell ($n_{\text{AlInP}} \sim 2.98$) is mitigated (two step graded) by employing the TiO_2 bi-layer ARC, resulting in the suppression of Fresnel reflection and thereby increasing photon absorption of the TJ solar cell. Fig. 1(c) shows the schematic of the OAD, which uses an electron-beam (e-beam) evaporator. A dense TiO_2 film having a high refractive index was obtained by setting the incident vapor flux angle (θ_{inc}) as 0° . Porous TiO_2 films having lower refractive indices were obtained by introducing air (porosity) within the deposited films by tilting the θ_{inc} up to 80° (*i.e.*, with respect to the substrate normal). Fig. 1(d) displays the cross-sectional view of the field-emission scanning electron microscope (FE-SEM, S-4700, Hitachi, Japan) images of a typical $\text{Ga}_{0.5}\text{In}_{0.5}\text{P}/\text{GaAs}/\text{Ge}$ TJ solar cell with the TiO_2 bi-layer ARC produced using OAD. On the top surface of the solar cell, the dense and porous TiO_2 films deposited at an θ_{inc} of 0° and 80° , respectively, are clearly observed. The porous TiO_2 film with inclined nanocolumnar structures is the result of the nuclei formation and self-shadowing effect.^{8,12} In the initial stages, evaporated adatoms condense onto the substrate and form nuclei, leaving the shadowed regions and preventing the following vapor flux from entering the shadowed region. Consequently, nanocolumnar structures which are inclined in the direction of the incident vapor flux are produced.^{8,12}

Prior to conducting theoretical calculations, the material properties of the oblique angle deposited TiO_2 films corresponding to θ_{inc} were investigated. Fig. 2(a) and (b) reveal the cross-sectional view of SEM images and the measured refractive indices (n) and extinction coefficients (k) of the TiO_2 films deposited at various θ_{inc} . It can be seen that the inclined angle of the deposited porous TiO_2 nanocolumnar structures become larger as the θ_{inc} increases, but smaller than θ_{inc} .^{9,16} The measured refractive indices and extinction coefficients using spectroscopic ellipsometry (UVISSEL, HORIVA, Japan) decrease due to the increased volume fraction of air within the deposited TiO_2 films with the increasing θ_{inc} . This result obviously indicates that the refractive index of an oblique angle deposited film can be engineered by adjusting the θ_{inc} . It is notable that the

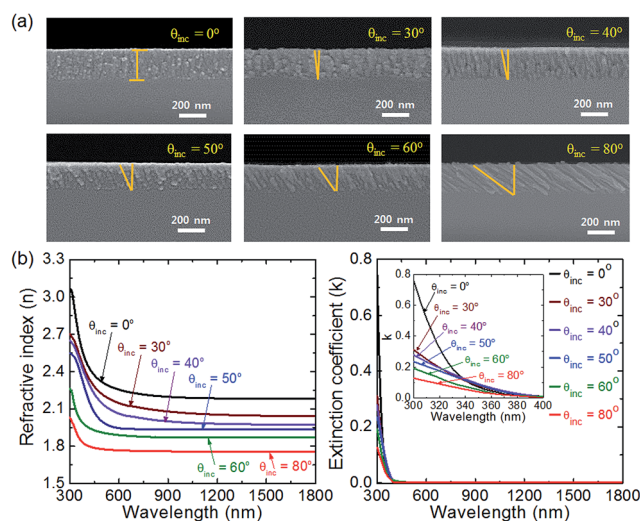


Fig. 2 (a) SEM images and (b) measured n and k of TiO_2 films deposited at various θ_{inc} . The inset is a magnified graph in the wavelength range 300–400 nm.

measured extinction coefficients of the deposited TiO_2 films are nearly zero for wavelengths above ~ 400 nm where most of the solar irradiance is distributed. This means that sunlight loss due to the TiO_2 ARC is not significant. From the refractive index measurement results, the porosity of the deposited TiO_2 film can be calculated using the following equation:¹¹

$$\text{Porosity}(\%) = \left(1 - \frac{n_{\text{film}}^2 - 1}{n_0^2 - 1} \right) \times 100 \quad (1)$$

where n_0 (≈ 2.52) is the refractive index of pore-free anatase TiO_2 ,¹⁷ and n_{film} is the measured refractive index of the deposited TiO_2 film. The calculated porosity of the TiO_2 films is presented in Table 1. As expected, the calculated porosity of the TiO_2 films was increased from 24.1% to 61.5% as the θ_{inc} increased from 0° to 80° because of the increased volume fraction of air inside the TiO_2 films.

Fig. 3(a) displays schematic illustrations and the refractive index profiles of (i) $\text{Ga}_{0.5}\text{In}_{0.5}\text{P}/\text{GaAs}/\text{Ge}$ (1.84/1.42/0.67 eV), (ii) $\text{Ga}_{0.51}\text{In}_{0.49}\text{P}/\text{Ga}_{0.96}\text{In}_{0.04}\text{As}/\text{Ga}_{0.37}\text{In}_{0.63}\text{As}$ (1.83/1.34/0.9 eV), and (iii) $\text{Ga}_{0.35}\text{In}_{0.65}\text{P}/\text{Ga}_{0.83}\text{In}_{0.17}\text{As}/\text{Ge}$ (1.67/1.18/0.67 eV) TJ solar cells which can be found in the literature.^{1,18–21} They have different combinations of materials, leading to different bandgap energy combinations (*i.e.*, different light absorption

ranges) and refractive index profiles. Fig. 3(b) shows the contour plots of calculated solar-weighted absorption (SWA) corresponding to the main absorption wavelength ranges of each subcell and the thickness of the dense and porous TiO_2 films which were deposited at an θ_{inc} of 0° and 80° , respectively. Optical simulation based on the rigorous coupled-wave analysis (RCWA) method was performed to obtain light absorption of the three different TJ solar cells with TiO_2 bi-layer ARCs to calculate the SWA.²² Then, by considering the solar spectrum and the absorption spectrum of each subcell, the SWA was calculated using the following equation:⁴

$$\text{SWA} = \frac{\int F(\lambda)A(\lambda)d\lambda}{\int F(\lambda)d\lambda} \quad (2)$$

where $F(\lambda)$ is the photon flux in the air mass 1.5 global (AM 1.5G) spectrum and $A(\lambda)$ is the calculated absorption.²³ For the RCWA simulation, the refractive indices of the compound semiconductor materials used were referenced,²⁴ and the step-grade layers were considered to be transparent layers.^{18,19} The net photocurrent in the $\text{Ga}_{0.5}\text{In}_{0.5}\text{P}/\text{GaAs}/\text{Ge}$ TJ solar cell is determined by the generated photocurrent in the $\text{Ga}_{0.5}\text{In}_{0.5}\text{P}$ top cell or GaAs middle cell.²⁴ This is because the Ge bottom cell, which has much smaller bandgap energy compared to the other subcells, generates much higher photocurrent than other subcells. For this reason, *i.e.*, current mismatching, the TiO_2 bi-layer ARC should be optimized to maximize the photon absorption both in the $\text{Ga}_{0.5}\text{In}_{0.5}\text{P}$ top cell and GaAs middle cell in order to enhance the net photocurrent, and thus improve the PCE of the TJ solar cell. Since the $\text{Ga}_{0.51}\text{In}_{0.49}\text{P}/\text{Ga}_{0.96}\text{In}_{0.04}\text{As}/\text{Ga}_{0.37}\text{In}_{0.63}\text{As}$ and $\text{Ga}_{0.35}\text{In}_{0.65}\text{P}/\text{Ga}_{0.83}\text{In}_{0.17}\text{As}/\text{Ge}$ TJ solar cells are current

Table 1 Calculated porosity of deposited TiO_2 films for various θ_{inc} . Refractive indices of each material at ~ 600 nm are considered

θ_{inc}	0	30	40	50	60	80
n_{film}	2.25	2.14	2.07	1.95	1.9	1.75
Porosity (%)	24.1	33.1	38.6	47.6	51.2	61.5

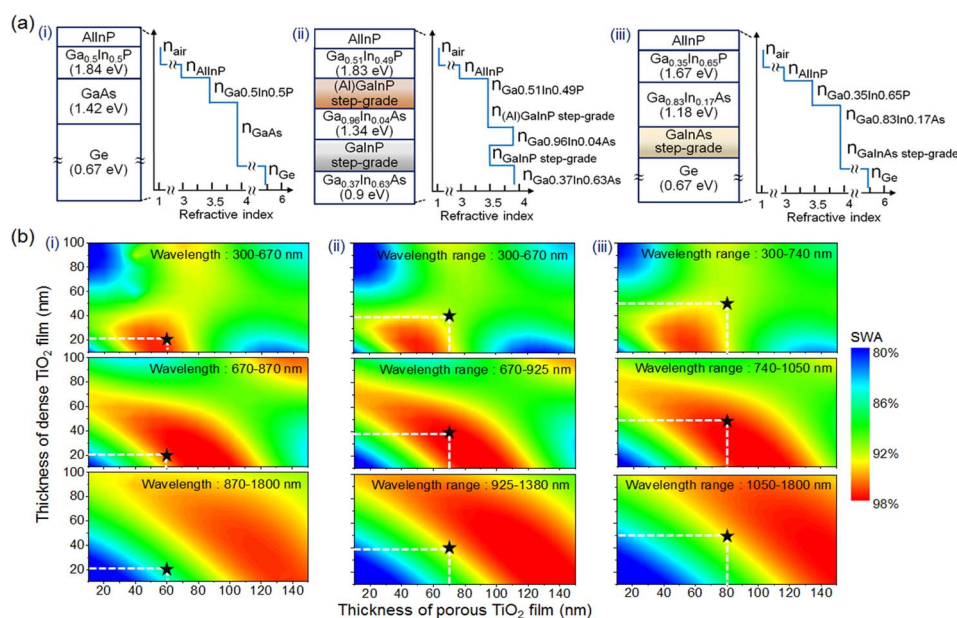


Fig. 3 (a) Schematic illustrations of cell designs and refractive index profiles of the three different TJ solar cells of (i) $\text{Ga}_{0.5}\text{In}_{0.5}\text{P}/\text{GaAs}/\text{Ge}$, (ii) $\text{Ga}_{0.51}\text{In}_{0.49}\text{P}/\text{Ga}_{0.96}\text{In}_{0.04}\text{As}/\text{Ga}_{0.37}\text{In}_{0.63}\text{As}$, and (iii) $\text{Ga}_{0.35}\text{In}_{0.65}\text{P}/\text{Ga}_{0.83}\text{In}_{0.17}\text{As}/\text{Ge}$. (b) Contour plots of the calculated SWAs of the TJ solar cells corresponding to the main absorption wavelength ranges of each subcell, and the thickness of dense ($n_{\text{dense}} \text{TiO}_2 \sim 2.25$) and porous ($n_{\text{porous}} \text{TiO}_2 \sim 1.75$) TiO_2 films.

Table 2 Optimum thickness of the TiO₂ bi-layer consisting of dense and porous TiO₂ films for various TJ solar cells

TiO ₂ bi-layer	Ga _{0.5} In _{0.5} P/GaAs/Ge	Ga _{0.51} In _{0.49} P/Ga _{0.96} In _{0.04} As/Ga _{0.37} In _{0.63} As ^{18,19}	Ga _{0.35} In _{0.65} P/Ga _{0.83} In _{0.17} As/Ge ^{20,21}
Dense ($n \sim 2.25$)/porous TiO ₂ ($n \sim 1.75$)	20/60 nm	40/70 nm	50/80 nm
Dense ($n \sim 2.4$)/porous TiO ₂ ($n \sim 1.5$)	40/80 nm	50/100 nm	50/80 nm

matched structures, the TiO₂ bi-layer ARC should be designed to identically enhance photocurrents in three subcells simultaneously. From the SWA calculation results, TiO₂ bi-layer ARCs consisting of 20/60, 40/70, and 50/80 nm-thick dense and porous TiO₂ films having refractive indexes of $n_{\text{dense TiO}_2} \sim 2.25$ and $n_{\text{porous TiO}_2} \sim 1.75$ at ~ 600 nm were considered to be an optimum antireflective structure for effectively enhancing the net photocurrent (*i.e.*, PCE) of the Ga_{0.5}In_{0.5}P/GaAs/Ge, Ga_{0.51}In_{0.49}P/Ga_{0.96}In_{0.04}As/Ga_{0.37}In_{0.63}As, and Ga_{0.35}In_{0.65}P/Ga_{0.83}In_{0.17}As/Ge TJ solar cells, respectively. We also carried out additional calculations using TiO₂ bi-layer ARCs consisting of more dense TiO₂ ($n_{\text{dense TiO}_2} \sim 2.4$) and porous TiO₂ ($n_{\text{porous TiO}_2} \sim 1.5$) films which can be found in the literature.¹¹ The optimum thicknesses of TiO₂ bi-layer ARCs for the three representative types of TJ solar cells are presented in Table 2.

In this study, we verified the effect of the finely designed TiO₂ bi-layer ARC on the PCE improvement of the TJ solar cells by fabricating Ga_{0.5}In_{0.5}P/GaAs/Ge TJ cells. The cells were monolithically grown on a p-type Ge substrate by metal-organic chemical vapor deposition system. TJ solar cells consisting of a 0.7 μm -thick Ga_{0.5}In_{0.5}P, 3.65 μm -thick GaAs, and 350 μm -thick Ge subcells and a 30 nm-thick AlInP window layer without the ARC layer were prepared using the following fabrication process. A Au/Ge/Ni/Au (20/50/10/300 nm) front metal electrode was deposited using an e-beam evaporator on a GaAs contact layer after removing the native oxide using diluted HCl solution. The undesirable contact layer, except the one underneath the front electrode area, was selectively removed using the chemical etching method. The photolithography process was carried out to form a mesa pattern and then a multi-step chemical etching process was performed to etch the solar cell structure onto the p-type Ge substrate. After forming a Ti/Pt/Au (20/20/300 nm) back metal electrode on the rear side of the TJ solar cell, the sample was annealed using a rapid thermal annealing system. After that, an optimum TiO₂ bi-layer ARC consisting of a 20 nm-thick dense TiO₂ film followed by a 60 nm-thick porous TiO₂ film was deposited onto the surface of the TJ solar cell using OAD at an θ_{inc} of 0° and 80°, respectively. To prevent the deposition of TiO₂ onto metal busbars, the metal busbars were screened before depositing the TiO₂ films. For comparison, a TJ solar cell with an optimum 55 nm-thick dense TiO₂ single-layer ARC was also fabricated.

Results and discussion

Photographs of the fabricated TJ solar cells without and with optimum TiO₂ single- and bi-layer ARC are displayed in Fig. 4(a). The TJ solar cell with the TiO₂ bi-layer ARC appears

nearly black because of its superior antireflection ability. In contrast, the cells without ARC and with a TiO₂ single-layer ARC show a gray and deep blue surface color due to their relatively poor antireflection property. Fig. 4(b) shows the reflectance spectra of the TJ solar cells. It can be obviously observed that the TJ solar cell with the optimum TiO₂ bi-layer ARC has lower light reflection than the other solar cells over the entire wavelength range. The summarized solar-weighted reflectance (SWR)⁶ values of the three TJ solar cells corresponding to the main absorption spectrum of each subcell are shown in Table 3. We also calculated the external quantum efficiency (EQE) of the TJ solar cells with and without TiO₂ ARC using a Silvaco ATLAS device simulator, as can be seen in Fig. 4(c). For an accurate EQE calculation, Shockley–Read–Hall recombination, Fermi–Dirac statistics, bandgap narrowing effect, and non-local tunnelling effect were considered. The TJ solar cell with the TiO₂ bi-layer ARC exhibited an increased EQE compared to the cells without ARC and with a TiO₂ single-

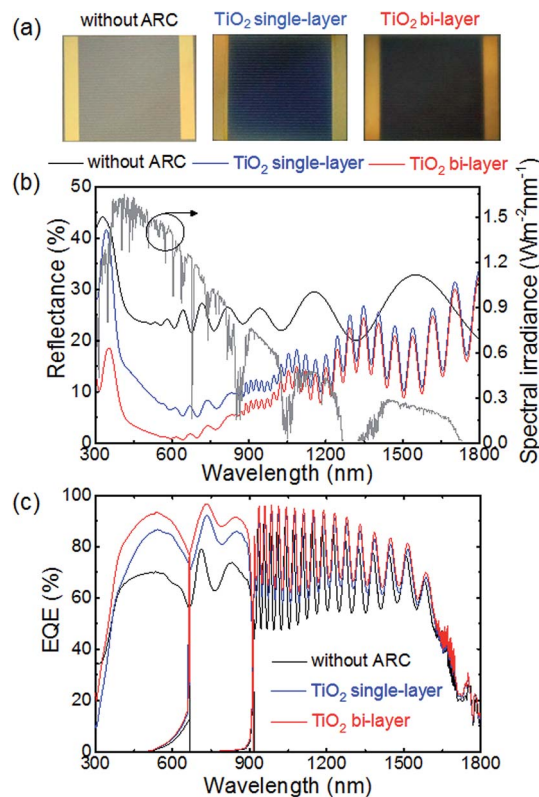


Fig. 4 (a) Photographs and (b) calculated reflection spectra and (c) EQE of the Ga_{0.5}In_{0.5}P/GaAs/Ge TJ solar cells without ARC, and with the optimum TiO₂ single- and bi-layer ARC.

Table 3 Calculated SWRs of the Ga_{0.5}In_{0.5}P/GaAs/Ge TJ solar cells without and with the optimum TiO₂ single- and bi-layer ARC corresponding to the main absorption wavelength range of each subcell

Wavelength (nm)	Without ARC (%)	TiO ₂ single-layer (%)	TiO ₂ bi-layer (%)
300–670	26.60	11.76	3.36
670–870	24.43	7.68	3.17
870–1800	26.11	15.44	12.73

layer ARC. In particular, the EQE improvement was prominent in the absorption wavelength ranges of the Ga_{0.5}In_{0.5}P and GaAs subcells, which determine the net photocurrent of the TJ solar cell, due to the precisely designed TiO₂ bi-layer ARC for suppressing the reflection loss in that wavelength range. Hence it is expected that the TJ solar cell with a TiO₂ bi-layer ARC may have an enhanced net photocurrent compared to other solar cells.

We confirmed the photocurrent and PCE enhancement of the TJ solar cell with the TiO₂ bi-layer ARC by measuring current density–voltage (*J*–*V*) characteristics using a solar simulator (Sol3A, Oriel, USA) under one-sun of AM 1.5G illumination at room temperature. Fig. 5 shows the measured *J*–*V* curves of the fabricated TJ solar cells having an active area of 0.2858 cm². The TJ solar cell with the TiO₂ bi-layer ARC exhibited a short-circuit current (*J*_{sc}) of 14.60 mA cm^{−2} which was a 29.7% and 8.7% enhanced *J*_{sc} compared to that without ARC (11.26 mA cm^{−2}) and with a TiO₂ single-layer ARC (13.43 mA cm^{−2}), respectively, because of the increased photon absorption as confirmed in Fig. 4(c). The open-circuit voltage (*V*_{oc}) of the TJ solar cells with ARCs was slightly increased, probably owing to the increased *J*_{sc}. This can be understood by the following equation:¹³

$$V_{oc} = \frac{E_g}{q} + \frac{NkT}{q} \ln(J_{sc}) - \frac{NkT}{q} \ln(J_0) \quad (3)$$

where *E*_g is the energy bandgap, *N* is the ideal factor, *kT/q* is the thermal voltage and *J*₀ is the saturation current density. It is observed that the fill factor (FF) of the TJ solar cells with TiO₂ ARC was also slightly increased. This presumably may be due to the surface passivation effect provided by the TiO₂ ARC. Overall,

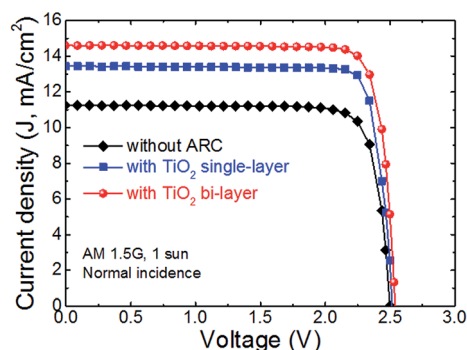


Fig. 5 Current density–voltage curves of Ga_{0.5}In_{0.5}P/GaAs/Ge TJ solar cells without and with optimum TiO₂ single- and bi-layer ARC.

the TJ solar cell with TiO₂ bi-layer ARC exhibited an enhanced PCE of 31.6% compared to that without ARC (23.8%) and with a TiO₂ single-layer ARC (29.1%), respectively. These results clearly show that the precisely designed TiO₂ bi-layer ARC with excellent antireflection properties can effectively enhance the net photocurrent and the PCE of TJ solar cells. The summarized characteristics of the TJ solar cells with and without TiO₂ ARC are presented in Table 4.

The sun's altitude changes during the day. Thus, the incident angle-dependent PCE of a solar cell is important to ensure the stable generation of solar electricity during the daytime. The measured incident angle-dependent PCE and *J*_{sc} of the TJ solar cells without ARC and with optimum TiO₂ single- and bi-layer ARC are plotted in Fig. 6. It is noteworthy that the TJ solar cell with the TiO₂ bi-layer ARC exhibited the highest PCE for the entire angle of incidence (AOI, *θ*_i) among the three different cells. As the AOI was varied from 20° to 60°, the PCE of the solar cells without ARC and with TiO₂ single- and bi-layer decreased from 22.6% to 10.9%, 28.2% to 13.5%, and 31.3% to 15.2%, respectively. The efficiency drop is predominantly due to the decreased *J*_{sc} (11.22 to 5.86 mA cm^{−2}, 13.53 to 7.36 mA cm^{−2}, and 14.70 to 8.20 mA cm^{−2} for the cells without and with TiO₂ single- and bi-layer ARC, respectively) with increasing AOI from 20° to 60°. Meanwhile, the decrease in *J*_{sc} can be attributed to the decline in incident sunlight into the solar cell proportional to cos *θ*_i as well as increased surface reflection loss with an increase in the AOI. Although incident angle-dependent *V*_{oc} and FF were slightly decreased 0.157 ± 0.059 V and 3.93 ± 1.58%, respectively, as the AOI increased from 20° to 60°, these changes did not much affect the incident angle-dependent PCE of the TJ solar cells.

Table 4 Summarized characteristics of the Ga_{0.5}In_{0.5}P/GaAs/Ge TJ solar cells without and with optimum TiO₂ single- and bi-layer ARC

Solar cell	<i>V</i> _{oc} (V)	<i>J</i> _{sc} (mA cm ^{−2})	FF (%)	PCE (%)
Without ARC	2.512	11.26	84.2	23.8
TiO ₂ single-layer	2.527	13.43	85.6	29.1
TiO ₂ bi-layer	2.538	14.60	85.3	31.6

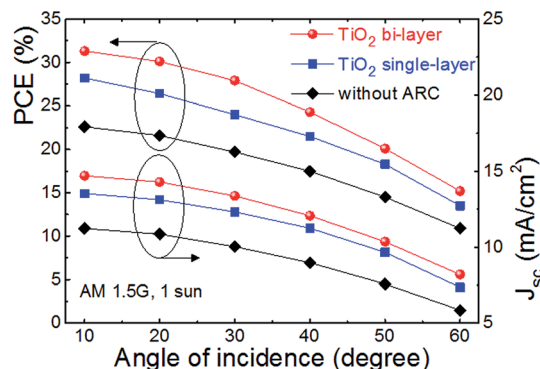


Fig. 6 Incident angle-dependent PCE and *J*_{sc} of the Ga_{0.5}In_{0.5}P/GaAs/Ge TJ solar cells without and with TiO₂ single- and bi-layer ARC.

Conclusions

Single-material TiO₂ bi-layer ARC produced by OAD were designed to maximize the PCE of three representative types of stacked TJ solar cells by taking into account the main absorption spectrum of each subcell and the solar irradiance. The Ga_{0.5}In_{0.5}P/GaAs/Ge TJ solar cell with an optimum TiO₂ bi-layer ARC having 20 nm-thick dense and 60 nm-thick porous TiO₂ films deposited at an θ_{inc} of 0° and 80°, respectively, exhibited considerably increased PCE of 31.6% compared to that of the cells without ARC (23.8%) and with a TiO₂ single-layer ARC (29.1%) under one-sun AM 1.5 G illumination. This is predominantly due to the enhanced J_{sc} with the TiO₂ bi-layer ARC, compared to the cells without ARC and with a TiO₂ single-layer ARC. The finely designed TiO₂ bi-layer ARC has superior antireflection properties which enhances photon absorption in the current-limiting subcells (*i.e.*, Ga_{0.5}In_{0.5}P and GaAs subcells). The TJ solar cell with the TiO₂ bi-layer ARC also exhibited a higher incident angle-dependent PCE than other solar cells in the AOI range of 20° to 60°. These results showed the great potential of versatile single-material graded refractive index ARC for effectively improving the PCE of various MJ solar cells without material selection issues for ARC.

Acknowledgements

This work was supported by the National Research Foundation of Korea (NRF) grant funded by the Korea government (MEST) (no. 2011-0017606).

Notes and references

- 1 D. J. Friedman, *Curr. Opin. Solid State Mater. Sci.*, 2010, **14**, 131–138.
- 2 P. Yu, M. Y. Chiu, C. H. Chang, C. Y. Hong, Y. L. Tsai, H. V. Han and Y. R. Wu, *Prog. Photovoltaics*, 2014, **22**, 300–307.
- 3 J. Tømmila, V. Polojärvi, A. Aho, A. Tukiainen, J. Viheriälä, J. Salmi, A. Schramm, J. M. Kontio, A. Turtianiene, T. Niemi and M. Guina, *Sol. Energy Mater. Sol. Cells*, 2010, **94**, 1845–1848.
- 4 C. I. Yeo, E. K. Kang, S. K. Lee, Y. M. Song and Y. T. Lee, *IEEE Photonics J.*, 2014, **6**, 8400209.
- 5 C. N. Eisler, Z. R. Abrams, M. T. Sheldon, X. Zhang and H. A. Atwater, *Energy Environ. Sci.*, 2014, **7**, 3600–3605.
- 6 C. I. Yeo, J. H. Kwon, S. J. Jang and Y. T. Lee, *Opt. Express*, 2012, **20**, 19554–19562.
- 7 J. Q. Xi, M. F. Schubert, J. K. Kim, E. F. Schubert, M. Chen, S. Y. Lin, W. Liu and J. A. Smart, *Nat. Photonics*, 2007, **1**, 176–178.
- 8 J. J. Steele and M. J. Brett, *J. Mater. Sci.: Mater. Electron.*, 2007, **18**, 367–379.
- 9 S. J. Jang, Y. M. Song, C. I. Yeo, C. Y. Park, J. S. Yu and Y. T. Lee, *Opt. Express*, 2011, **19**, A108–A117.
- 10 J. W. Leem and Y. T. Lee, *Opt. Express*, 2011, **19**, A258–A268.
- 11 P. Mao, F. Sun, H. Yao, J. Chen, B. Zhao, B. Xie, M. Ham and G. Wang, *Nanoscale*, 2014, **6**, 8177–8184.
- 12 P. Yu, C. H. Chang, C. H. Chiu, C. S. Yang, J. C. Yu, H. C. Kuo, S. H. Hsu and Y. C. Chang, *Adv. Mater.*, 2009, **21**, 1618–1621.
- 13 L. K. Yeh, K. Y. Lai, G. J. Lin, P. H. Fu, H. C. Chang, C. A. Lin and J. H. He, *Adv. Energy Mater.*, 2011, **1**, 506–510.
- 14 B. S. Richards, *Prog. Photovoltaics*, 2004, **12**, 253–281.
- 15 E. Shi, H. Li, L. Yang, L. Zhang, Z. Li, P. Li, Y. Shang, S. Wu, X. Li, J. Wei, K. Wang, H. Zhu, D. Wu, Y. Fang and A. Cao, *Nano Lett.*, 2013, **13**, 1776–1781.
- 16 Y. Zhong, Y. C. Shin, C. M. Kim, B. G. Lee, E. H. Kim, Y. J. Park, K. M. A. Sobahan, C. K. Hwangbo, Y. P. Lee and T. G. Kim, *J. Mater. Res.*, 2008, **23**, 2500–2505.
- 17 W. D. Kingery, H. K. Bowen and D. R. Uhlmann, *Introduction to Ceramics*, Wiley, New York, 1976, pp. 650–651.
- 18 J. F. Geisz, D. J. Friedman, J. S. Ward, A. Duda, W. J. Olavarria, T. E. Moriarty, J. T. Kiehl, M. J. Romero, A. G. Norman and K. M. Jones, *Appl. Phys. Lett.*, 2008, **93**, 123505.
- 19 J. F. Geisz, A. X. Levander, A. G. Norman, K. M. Jones and M. J. Romero, *J. Cryst. Growth*, 2008, **310**, 2339–2344.
- 20 W. Guter, J. Schöne, S. P. Philipps, M. Steiner, G. Siefer, A. Wekkeli, E. Welser, E. Oliva, A. W. Bett and F. Dimroth, *Appl. Phys. Lett.*, 2009, **94**, 223504.
- 21 F. Dimroth, R. Beckert, M. Meusel, U. Schubert and A. W. Bett, *Prog. Photovoltaics*, 2001, **9**, 165–178.
- 22 M. G. Moharam and T. K. Gaylord, *J. Opt. Soc. Am.*, 1981, **71**, 811–818.
- 23 NREL's AM1.5 Standard Dataset: <http://rredc.nrel.gov/solar/spectra/am1.5/>, accessed 17 January 2014.
- 24 SOPRA, <http://www.sopra-sa.com>, accessed 1 September 2013.